Rare Metal Materials and Engineering
Volume 53, Issue 8, August 2024
Available online at www.rmme.ac.cn

Science Press

Cite this article as: Zhou Bokai, Liu Xin, Li Shen, et al. Microstructure Evolution of 690 TT Heat Transfer Tube Under Impact Slip Dual-Axis Fretting Corrosion in High Temperature and High Pressure Water Environment[J]. Rare Metal Materials and Engineering, 2024, 53(08): 2156-2166. DOI: 10.12442/j.issn.1002-185X.E20230046.

ARTICLE

Microstructure Evolution of 690 TT Heat Transfer Tube Under Impact Slip Dual-Axis Fretting Corrosion in High Temperature and High Pressure Water Environment

Zhou Bokai, Liu Xin, Li Shen, Hu Yong

China Institute of Atomic Energy, Beijing 102413, China

Abstract: The service water environment of high temperature and high pressure was simulated for the steam generator heat transfer tube of pressurized water reactor. 690 TT alloy tube and 405 SS plate were used to form the friction pair for impact slip dual-axis fretting corrosion experiments. The microstructure evolution of 690 TT alloy tube during dual-axis impact slip fretting corrosion was investigated. White light interferometer, scanning electron microscope, transmission electron microscope, and Raman spectrum were used to investigate the microstructure and abrasive products of the abraded surface and near-surface. Results indicate that within 10^5 cycles, the wear mechanism of 690 TT alloy tube is mainly adhesive wear accompanied by material transfer. With the increase in cycles from 5×10^5 to 2×10^6, the wear mechanism of 690 TT alloy tube is mainly crack initiation, propagation, and delamination. In terms of microstructure evolution, mixed layer exists under the three body layer in the cross-section microstructure of samples after 10^5 cycles. The microstructures of samples after 5×10^5 and 2×10^6 cycles show slight difference and present a tribological transfer structure layer with thickness of about 500 nm. Additionally, the microstructure evolution enters the stable stage.

Key words: 690 TT alloy; impact slip fretting corrosion; microstructure evolution

Steam generator (SG) is a crucial component in pressurized water reactors, and the safe operation of SG heat transfer tubes is essential for the overall reactor performance. The research on the microstructure evolution of 690 TT heat transfer tubes during impact slip dual-axis fretting corrosion in high temperature and high pressure water environment is of great significance.

690 TT alloy, as an austenitic nickel-based alloy, is selected to manufacture SG heat transfer tubes due to its excellent resistance against stress corrosion cracking. However, the continuous small displacements, sliding, and collisions between the heat transfer tubes and support plates or anti-vibration strips may lead to thinning and fracture of the tube wall.

The physical and chemical factors, such as temperature, amplitude, frequency, dissolved oxygen and hydrogen concentrations, and pH value[1–6], have impact on the wear properties. Additionally, the impact wear under room temperature and atmospheric pressure air conditions has been widely researched. However, the impact slip dual-axis fretting corrosion in high temperature and high pressure water environments[7–8] is rarely studied.

Therefore, in this research, the service environment was simulated and the effect of the number of cycles on fretting corrosion was discussed under high temperature and high pressure water environment. The microstructure evolution was investigated to analyze the damage mechanism and behavior of 690 TT alloy heat transfer tubes under these specific conditions. Besides, a predictive model was established to predict and accurately evaluate the wear degree. Particularly, this research analyzed the entry process of stable stage in the wear process. Studying the microstructure evolution is crucial for the development and accuracy of prediction model in the wear process. Thus, this research simulated the actual environment in the reactor and studied the microstructure evolution of 690 TT alloy tube during impact slip wear under high temperature and high pressure conditions, which is essential to understand the mechanism and improve the

Received date: October 31, 2023
Foundation item: National Key Research and Development Program of China (2019YFB1900904)
Corresponding author: Hu Yong, Ph. D., Researcher, China Institute of Atomic Energy, Beijing 102413, P. R. China, E-mail: huyong@ciae.ac.cn

performance with service life of SG heat transfer tubes, ultimately contributing to the safe efficient operation of pressurized water reactors.

1 Experiment

690 TT alloy is one of the most commonly used materials for the manufacture of heat transfer tubes in SGs, and the racks of heat transfer tubes are usually made of 405 SS material. Therefore, in the wear experiments, nuclear-grade commercial 690 TT alloy tubes and 405 SS plates were selected as wear pair. The chemical composition of 690 TT tube and 405 SS plate is provided in Table 1.

The 690 TT wear samples was cut into the ones with length of 15 mm, and the surface of 405 SS plate was polished. The samples were then washed with anhydrous ethanol and dried.

As shown in Fig.1, the wear pair was loaded and subjected to wear test, which simulated the conditions of dual-axis fretting wear process during impact sliding in high temperature and high pressure water environments. Afterwards, the microstructure evolution of the 690 TT heat transfer tubes was observed by scanning electron microscope (SEM), transmission electron microscope (TEM), energy dispersive spectrometer (EDS), electron back-scattered diffractometer (EBSD), and focused ion beam (FIB) technique. The high-resolution TEM (HRTEM) coupled with selected area electron diffractometer (SAED) was also used for analysis.

This experiment was conducted in an autoclave to attain the high pressure conditions and a high-temperature sensor was used to ensure the high temperature conditions. The impact shaft and sliding shaft were driven by a servo motor, and a sealing ring was used at the connection between the shaft and the high pressure kettle to ensure the high pressure environment inside the autoclave.

Ammonia was used to adjust the pH value of the deionized water in the water tank to 10±0.05. Continuous bubbling of N_2 was employed to deoxygenate the water and control the dissolved oxygen value as 10±0.05 μg/L.

The temperature of the autoclave was controlled as 285 °C, and the back pressure valve was adjusted to increase the pressure inside the kettle to 8.6 MPa. Once the conditions inside the autoclave satisfied the set ones, the sliding displacement of the wear test was set as ±150 μm.

Throughout the testing period, a normal force of 0–80 N was applied to the 690 TT alloy tube using a normal loading system in a sine wave manner. Simultaneously, the 405 SS plate underwent reciprocating motion controlled by the lateral driving system at the testing frequency of 30 Hz.

Fig. 2 shows the FIB sample preparation process. After selecting a suitable location in the center area of the grinding mark and spraying a Pt protective layer, the slices at that location are extracted and gradually thinned on the sample rack.

Table 1 Chemical composition of 690 TT alloy tube and 405 SS plate (wt%)

Material	Ni	Cr	Fe	Mn	Ti	Al	C
690 TT	59.3	29.8	9.3	0.2	0.3	0.4	0.01
405 SS	0.3	13.1	85.3	0.7	-	0.1	0.056

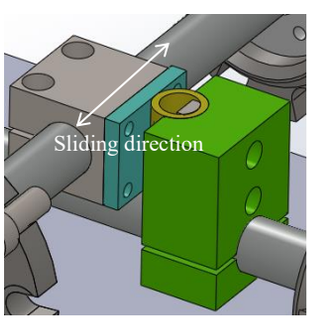

Fig.1 Schematic diagram of wear pair

2 Results and Discussion

2.1 Microstructure evaluation

As shown in Fig.3a, SEM images of the initial 690 TT alloy tube exhibit certain characteristics. Due to the high temperature annealing treatment, the alloy suffers carbide nucleation and growth along the interface between undissolved carbides and matrix. This phenomenon results in the production of a small number of relatively large precipitates within the crystal structure. Additionally, due to their supersaturated state, carbon atoms tend to gather near grain boundaries with higher free energy, which leads to the formation of small semi-continuous intergranular carbides along the grain boundaries of 690 TT alloy tube. The sizes of the intergranular carbide particles are on the order of several hundred nanometers. The random distribution of titanium nitride (TiN) can also be observed, which contributes to the resistance against stress corrosion cracking. As shown in Fig.3b, 405 SS plate presents the typical banded crystals.

Fig.4 displays EBSD images of 690 TT alloy tube and 405 SS plate. Within the original grain of 690 TT alloy tube, a significant number of annealing twins can be observed. This is attributed to the low stacking fault energy, which promotes twinning deformation during pipe rolling. Subsequent annealing processes lead to the formation of these annealing twins.

The grain size of the 690 TT alloy tube ranges from 10 μm to 70 μm, whereas that of the 405 SS plate ranges from 5 μm to 110 μm. Ref. [9] indicated that smaller grain sizes are associated with higher hardness and better wear resistance. In this case, the small grain sizes result in the low contact stress on the sample, which facilitates the formation of wear marks with subsurface tribological transfer structure (TTS). The layered microcracks generated by TTS are shorter in the grains of small sizes, compared with those in the grains of large sizes.

Due to the annealing treatment, the grain size distribution in the matrix of 690 TT alloy tube is uniform, and no significant difference can be observed in grain sizes between the sample

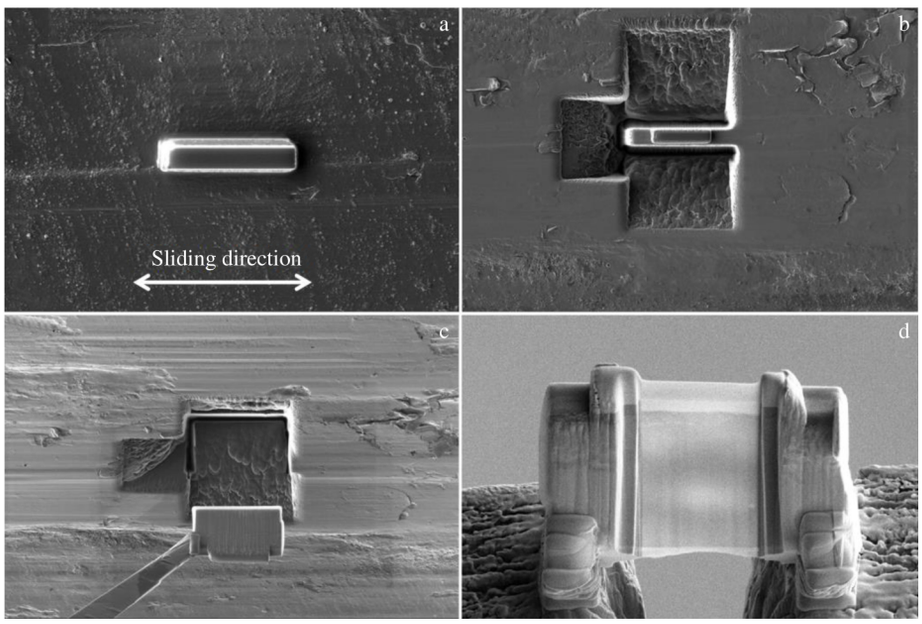

Fig.2 FIB sample preparation process: (a) spray coating protective layer; (b) rough cut; (c) extraction; (d) gradual thinning

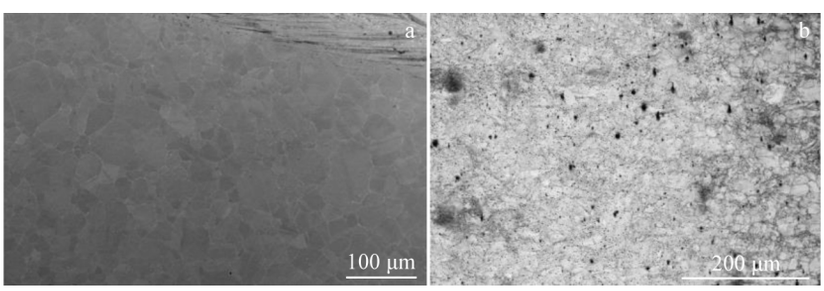

Fig.3 SEM images of initial grains in 690 TT alloy tube (a) and 405 SS plate (b)

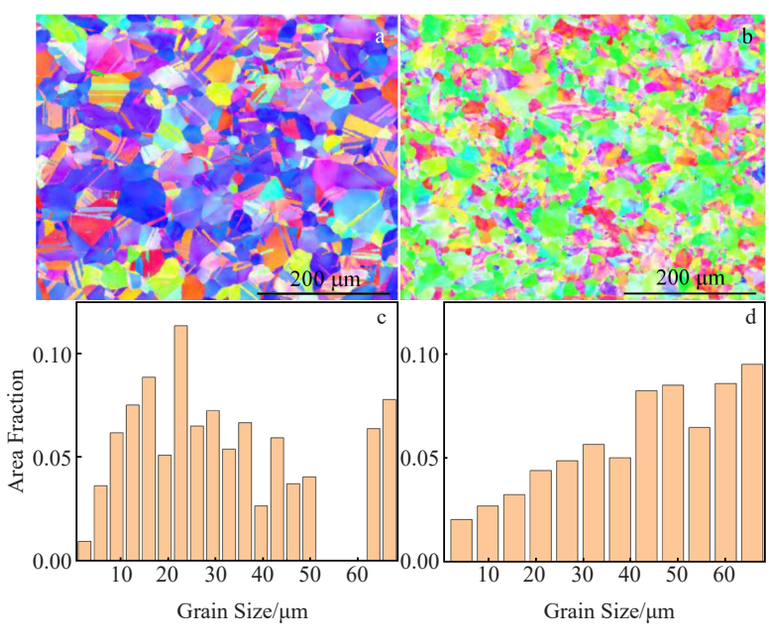

Fig.4 EBSD images (a–b) and grain size distributions (c–d) of 690 TT alloy tube (a, c) and 405 SS plate (b, d)

surface and the matrix. Consequently, the influence of grain size on wear is barely changed with the increase in wear depth.

2.2 Material surface friction and wear

Fig.5 presents the 3D profiles of wear marks on the surface

of 690 TT alloy tube and 405 SS plate after different cycles. To account for the uneven curvature of 690 TT alloy tube surface, a global bow removal method was employed to fit the sample. As shown in Fig. 5, distinct furrows appear, which result from the abrasive wear. Additionally, with the increase in the number of cycles, the wear marks on both 690 TT alloy tube and 405 SS plate are gradually widened, indicating greater material loss. EDS analysis shows that the content of Fe and O elements in the protrusions on both sides of the 690 TT alloy tube is significantly higher than that of the matrix. This suggests that the material in this area originates from the transfer of the 405 SS plate.

It can be observed that the contour of the wear marks in Fig. 5c – 5d and 5f is not uniform. This is mainly due to the uncertainty of the fretting process, during which the running posture of the friction pair constantly changes, resulting in severe wear at one end. From the macro perspective, the fact that the degree of wear on one side is more severe than that on the other side is attributed to the tilting of the workpiece during contact, resulting in a greater contact force at one end. However, with the wear process proceeding, the wear depth at the severely worn end is gradually deepened, and the pressure at each contact surface gradually reaches dynamic equilibrium, ultimately forming relatively uniform wear marks in the subsequent wear process. Considering that the wear process is not uniform in the practical situations, forward contact force was used in this research as an indicator to measure the wear degree instead of the pressure of a certain part. Additionally, the wear amount was also used as an indicator to measure the wear degree, which could efficiently evaluate the severity of wear.

Notably, visible protrusions of above 4 μm can be observed on the unworn surface on both sides of the wear mark. These protrusions may originate from the plastic deformation of the material in the center area of 690 TT tube due to abrasive wear or material transfer from the 405 SS plate.

Under the influence of adhesive wear, debris generated on the 405 SS plate adheres to the surface of 690 TT alloy tube. Subsequent squeezing motion causes the transferred material to move and accumulate along the sliding direction, resulting in protrusions on the surface. Material transfer occurs not only at the edge of the wear scar but also in the center wear area. The accumulation of material transfer leads to the elevation of the edge area of the wear scar, compared with other regions.

Fig. 6 shows the wear volumes of 690 TT tube after different cycles. Through calculation, for the samples after 10^5, 5×10^5, and 2×10^6 cycles, the average wear amount in every 10^4 cycles is 5.3×10^{-4}, 2.5×10^{-4}, and 2.9×10^{-4} mm^3, respectively. It can be seen that the average wear amount in every 10^4 cycles significantly decreases at first and then increases slowly. For the sample after 10^5 cycles, it mainly enters the running-in stage, which is an uneven stage in the wear process[12]. When the metals are in contact, only a small portion of the microconvex body is in direct contact with the surface, so the pressure at the microconvex contact point is sufficient to cause plastic deformation, greatly increasing the formation of abrasive particles and causing serious damage to the surface. Therefore, in the early stage of wear, the wear rate is very high. After the running-in stage, two small planes are in direct contact, smoothing the surface. At the same time, the dense triple body layer (TBL) formed by spinel oxide presents the lubrication function[16–17], effectively reducing the probability of abrasive particle formation and slowing down the wear rate.

Through the calculation of the average wear amount in samples after 5×10^5 and 2×10^6 cycles, it can be seen that there is a slow increasing trend in the wear rate during this process. This result suggests that the abrasion does not reach a stable state when the number of cycles is $10^5 - 5\times10^5$. In pure slip fretting, the wear rate typically slows down[7]; whereas in impact slip, the wear rate continues to increase. This is due to the impact effect. When the lubricant TBL is formed by the detached debris and metal oxides, its adhesion is not very strong. The impact process will cause the fall-off phenomenon of TBL attached to the contact surface, degrading the lubrication effect of TBL during the wear process and thus exacerbating wear. At the same time, cracks produced below the surface will be affected by impact, and the impact force of cyclic loading will cause the small bending moments for the metal above cracks accompanied by the formation and

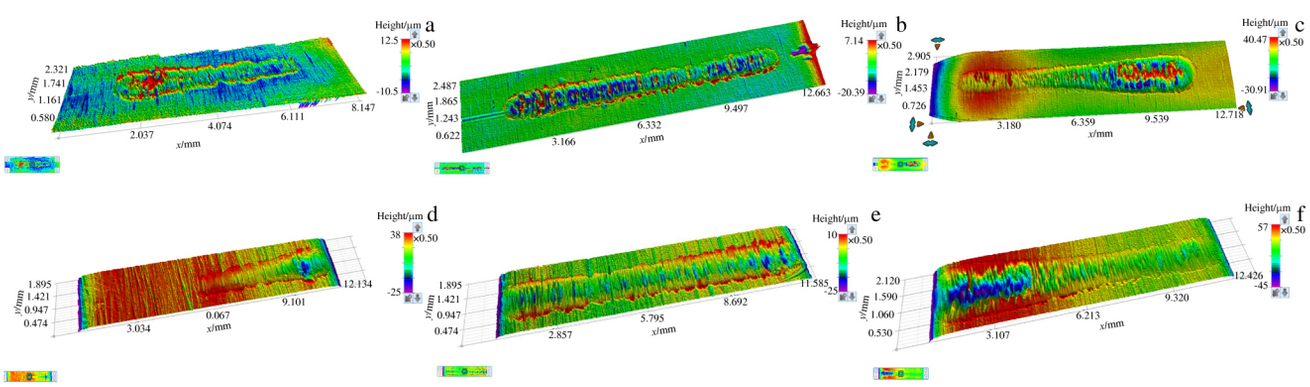

Fig.5 3D profiles of wear marks on surface of 690 TT alloy tube (a–c) and 405 SS plate (d–f) after different cycles: (a, d) 10^5 cycles, (b, e) 5×10^5 cycles, and (c, f) 2×10^6 cycles

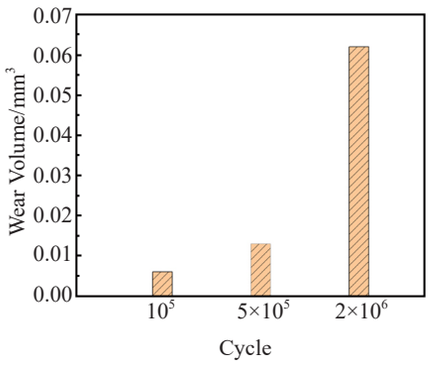

Fig.6 Wear volumes of 690 TT alloy tube after different cycles

accumulation of dislocations. The dislocation accumulation of a certain degree leads to the formation of metal fatigue fracture. Compared with pure sliding, the impact effect will accelerate the process of metal fatigue fracture above the cracks, so the wear rate presents a slow upward trend.

Considering the wear volume, it is important to note that subsequent wear cannot be perceived as a repetition of the previous wear process. To determine whether the process from 5×10^5 cycles to 2×10^6 cycles reaches a stable stage, further experiments with larger cycles are required for verification.

Fig. 7a – 7b display the wear depth (namely scar depth) profiles in the center section of the 690 TT alloy tube and 405 SS plate after different cycles, respectively. With the increase in cycles, both the wear depth and width are gradually increased. For the 690 TT alloy tube, the maximum wear depth is increased from 10 μm to 18 μm with the increase in

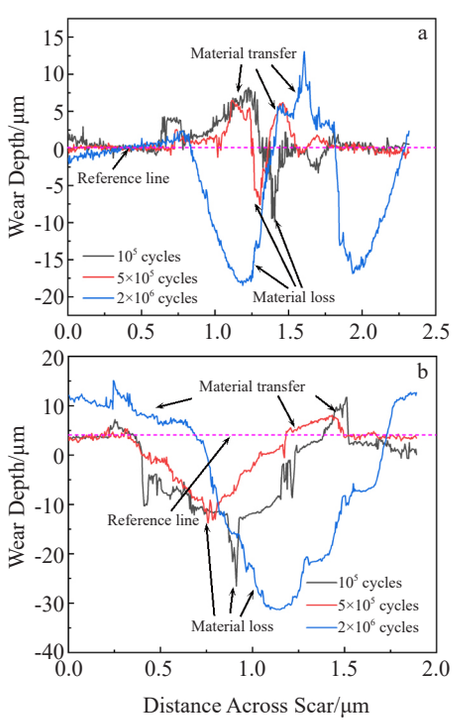

Fig.7 Wear depth profiles of 690 TT alloy tube (a) and 405 SS plate (b) after different cycles

the number of cycles from 10^5 to 2×10^6. The profile of the wear marks on the 690 TT alloy tube is influenced by the cross-section morphology of the wear marks on the friction pair and the stress distribution on the contact surface.

Comparing the maximum wear depth and wear volume, it is found that the results of 690 TT alloy tube are lower than those of 405 SS plate. Additionally, the material loss in the center area of the 690 TT alloy tube is relatively small, indicating the superior wear resistance, compared with the 405 SS plate. This can be attributed to the face-centered cubic crystal structure of the 690 TT alloy tube, which offers more sliding directions, compared with the body-centered cubic crystal structure of the 405 SS plate[10].

According to the adhesive wear theory, during the fretting process, softer materials tend to fracture and transfer onto the surface of harder materials, resulting in a W-shape wear depth profile on the 690 TT alloy tube. Furthermore, combined with EDS analysis, the Fe element content in the center area of the wear scar is significantly higher than that of the original 690 TT alloy tube. Therefore, it can be concluded that the protrusion in the center area originates from material transfer from the 405 SS plate. In contrast, the contour map of the wear depth on the 405 SS plate exhibits the typical U-shape.

2.3 Microscopic characterization and material analysis

Fig.8 presents SEM images of the 690 TT alloy tube surface after different cycles. It is evident that at lower cycles, the wear marks are narrower, but the cutting phenomena caused by abrasive wear and furrows can be observed. After 10^5 cycles, significant material transfer occurs on the metal surface, leading to the formation of furrows. This can be attributed to the uneven grinding process. During the initial contact between 690 TT alloy tube and 405 SS plate, only a small degree of microconvex contact occurs, resulting in severe abrasive wear and surface damage on the microconvex bodies. The high contact pressure induces plastic deformation on the metal surface, promoting the material transfer.

Material transfer becomes noticeable on the 690 TT alloy tube surface after 10^5 and 5×10^5 cycles, indicating the adhesive wear as the dominant wear mechanism. Fig. 8d reveals slight cracks and scratches on the metal surface after 10^5 cycles, but no distinct layering phenomenon can be observed. This is considered as the initial stage of crack initiation. Therefore, it is concluded that the adhesive wear is the primary wear mechanism at low cycles (10^5 cycles).

Fig. 9 displays SEM images and corresponding EDS analysis results of the 690 TT alloy tube surface after different cycles. It is observed that the content of Fe and O elements in the wear scar area initially decreases and then increases from the center. This phenomenon can be explained by the characteristics of wear process.

The center of the wear mark represents the total slip area, where the friction pair suffers the highest contact stress. This stress exceeds the elastic limit of the metal, resulting in relative sliding. Under the conditions of normal contact force and relative slip, material transfer and oxidation occur obviously, leading to the high content of Fe and O elements in

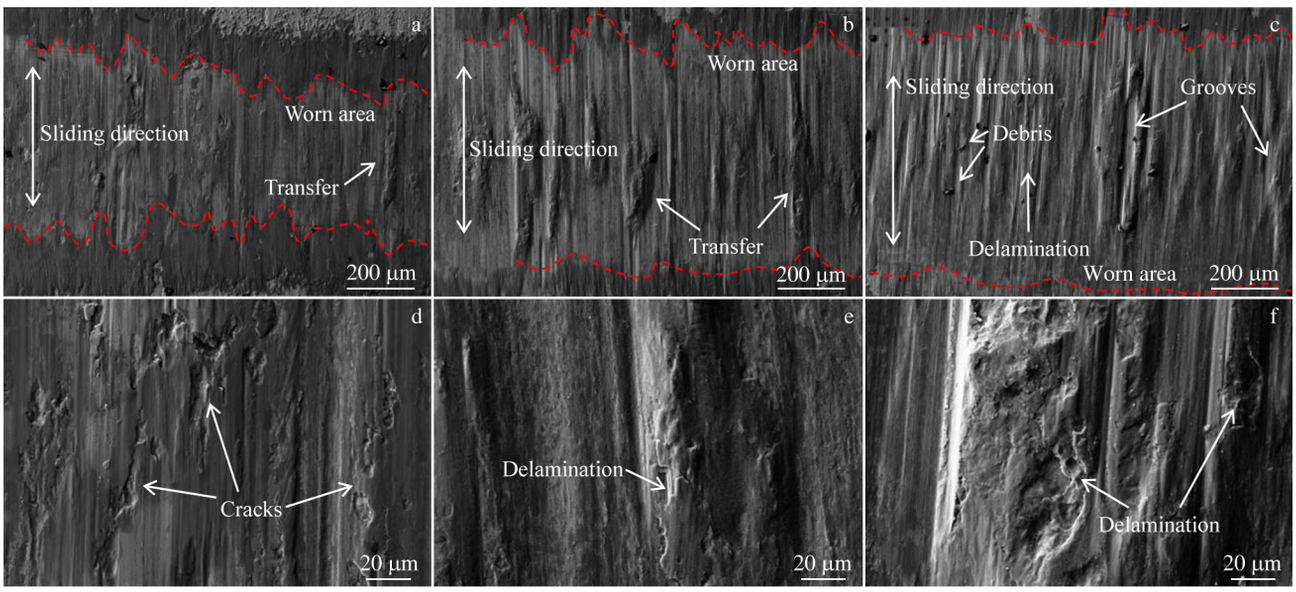

Fig.8 SEM surface morphologies of 690 TT alloy tube after 10^5 cycles (a, d), 5×10^5 cycles (b, e), and 2×10^6 cycles (c, f)

the central region.

On the outer side of the wear mark, the normal contact force is not as high as that in the central area, even contact exists, and it remains within the elastic limit of the metal. Therefore, only cyclic compression occurs without exceeding the elastic limit. However, the adhesion may still occur, and the material transferred from 405 SS plate moves outward under repeated stress compression, resulting in the stacking and oxidation of the transferred material. This stacking effect can also be observed in Fig. 5a–5c, as indicated by the higher position at the edge region of metal surface due to stacking.

As a result, in certain slip regions, the content of Ni and Cr increases, and the surface elements are similar to the elements of 690 TT alloy tube. However, in the edge region with material stacking, the content of Fe and O elements increases again.

Fig. 9p–9r show EDS line scanning results of line 1, line 2, and line 3 in Fig. 9a – 9c, respectively. At the edge of the material stacking area, it can be seen that the content of O element rapidly increases, whereas the content of Fe element increases slightly. This indicates that a large number of metal oxides are attached to the surface of wear marks, i.e., material transfer occurs.

Fig. 10 exhibits the Raman analysis of 690 TT alloy tube surface after different cycles. The observed shift peaks in the Raman spectra are primarily located at 665 and 675 cm^{-1}, whereas the weak peaks can be observed at 532 and 315 cm^{-1}.

By comparing the absorption peaks with those of standard oxides[11], it is determined that the main oxides present on the worn surface are Fe_3O_4 and spinel (Ni, Fe)(Fe, Cr)$_2O_4$ oxides.

However, due to the close proximity of the absorption peaks of specific spinel components, it is difficult to determine the exact type of spinel oxide.

Fig. 11 shows SEM cross-section images of 690 TT alloy tube after different cycles. As shown in Fig. 11a – 11b, no evident delamination or crack initiation can be observed in the worn section after 10^5 cycles. However, protrusions resulting from material transfer can be observed at the rear region, indicating that adhesive wear is the predominant damage mechanism within 10^5 cycles. Fig. 11c – 11e depict the cross-section images of wear marks on 690 TT alloy tube after 5×10^5 cycles. Numerous cracks are visible beneath the surface with width of approximately 1 μm and length of about 4 μm, extending downward at an angle of 30° along the surface. These cracks are formed due to repeated plastic shear of the material. The strain and intergranular stress do not accumulate on the material surface, ultimately leading to crack formation. During each half cycle, the relative motion direction of the friction pair changes, causing the transformation of compressive state inside the metal to the tensile state. As a result, the cracks are propagated parallel to the surface rather than penetrating the material. Therefore, it is inferred that the crack initiation and propagation are the primary damage mechanisms after approximately 5×10^5 cycles. Fig. 11f – 11g display the cross-section images of wear marks on the 690 TT alloy tube after 2×10^6 cycles. Clear delamination can be observed on the metal surface after 2×10^6 cycles, and the voids appear beneath the delamination. It was reported that under the influence of compressive and shear stresses, crack growth tends to terminate, preventing further expansion into the substrate[12–13]. The thickness of the surface layer is approximately 1 μm. This layer is formed parallel to the surface. After reaching a certain length, the layer intersects with other cracks, resulting in the delamination. EDS line scanning results reveal that the content of O element is high, indicating the formation of TBL through the aggregation of the peeled layer on the metal surface after oxidation.

Fig. 12 shows bright field TEM images and EDS mappings of the samples prepared for FIB in the center area of wear marks of 690 TT alloy tube. The microstructure of the metal

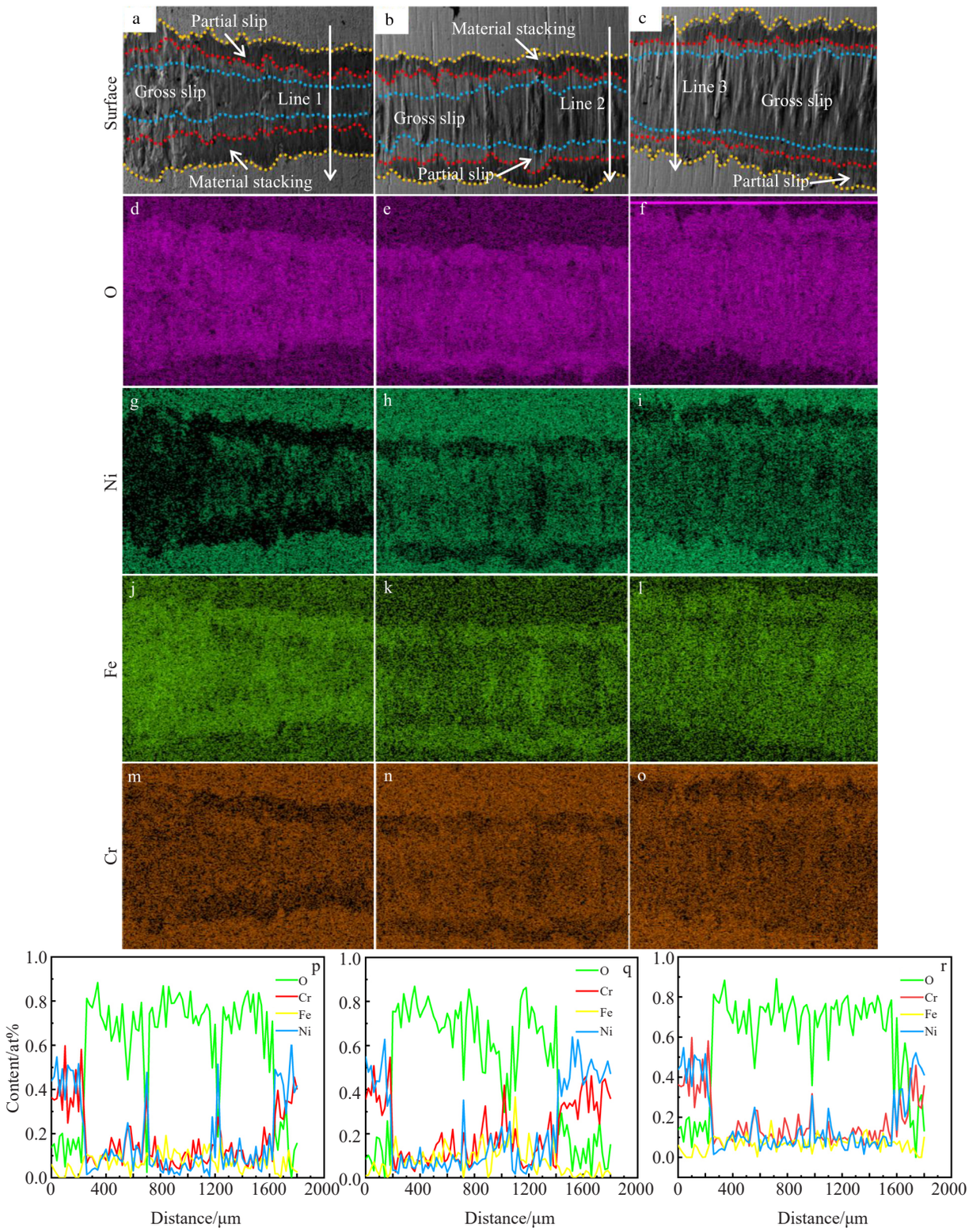

Fig.9 SEM images (a–c), EDS mappings (d–o), and EDS line scanning results (p–r) of 690 TT alloy tube surface after 10^5 cycles (a, d, g, j, m, p), 5×10^5 cycles (b, e, h, k, n, q), and 2×10^6 cycles (c, f, i, l, o, r)

surface after fretting corrosion can be divided into TBL, TTS, and general deformation layer (GDL), which is consistent with the results in Ref.[14–15]. The surface of TBL is rich in Fe and O elements, indicating that TBL is mainly formed by oxidation and extrusion of materials transferred from 405 SS plate. According to Fig. 12a – 12b, a mixed layer of material with high transverse Fe element content can be observed under the three body layer, 690 TT alloy matrix is under TBL in the sample after 10^5 cycles, and TBL thickness is about 1 μm. TBL may be formed from the beginning of the cycles. At

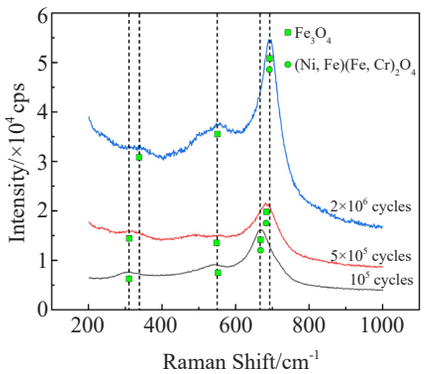

Fig.10 Raman analysis of 690 TT alloy tube surface after different cycles

the beginning of the cycles, there is no difference between the metal grains in the 690 TT alloy tube surface and the matrix, both of which are composed of larger equiaxed grains. Their hardness and strength are much lower than those of TTS layer with fine grain structure, hindering the material expansion along depth. The Fe-rich material on the 405 SS plate transfers to the surface of 690 TT alloy tube through adhesive wear, and it is mixed with more fragile large-sized grains which have not yet been formed into TTS layer to form a mixed layer. With the cycles proceeding, it moves laterally and is crushed to form a strip-like morphology. Under the mixing layer, TTS layer with thickness of approximately 2 μm can be observed, indicating that at this stage, TTS layer rapidly forms.

According to Fig. 12c–12d, no Fe, Ni, or Cr doped mixing layer exists in the sample after 5×10^5 cycles, because the material in the mixing layer is crushed, peels off, or enters the TBL with the cycles proceeding, and TTS layer and TBL come into direct contact. There are a large number of fine grains in TTS layer, which increases the difficulty of dislocation generation and the resistance against continuous sliding. Therefore, TTS layer has greater hardness and strength, which can effectively organize the downward extension and expansion of materials in TBL. Therefore, the mechanism of adhesive wear gradually fails. In GDL below TTS layer, transverse stacking defects can also be observed, and metal grains gradually separate from larger equiaxed grains in the matrix, forming TTS layer.

Compared with Fig. 12a, TBL, TTS layer, and GDL in Fig. 12c show significant thinning effect. Based on Fig. 11g, it can be seen that there are gaps between TBL and metal surface, because TBL is mainly formed by detached wear debris and metal oxide debris with poor adhesion ability and insufficient adhesion to the metal surface. The high-frequency fretting process has strong randomness, so it is believed that the thinning of TBL is not universal. Accidental phenomenon occurs at the selected location during FIB sample preparation. In the early stage of wear process within 10^5 cycles, the metal

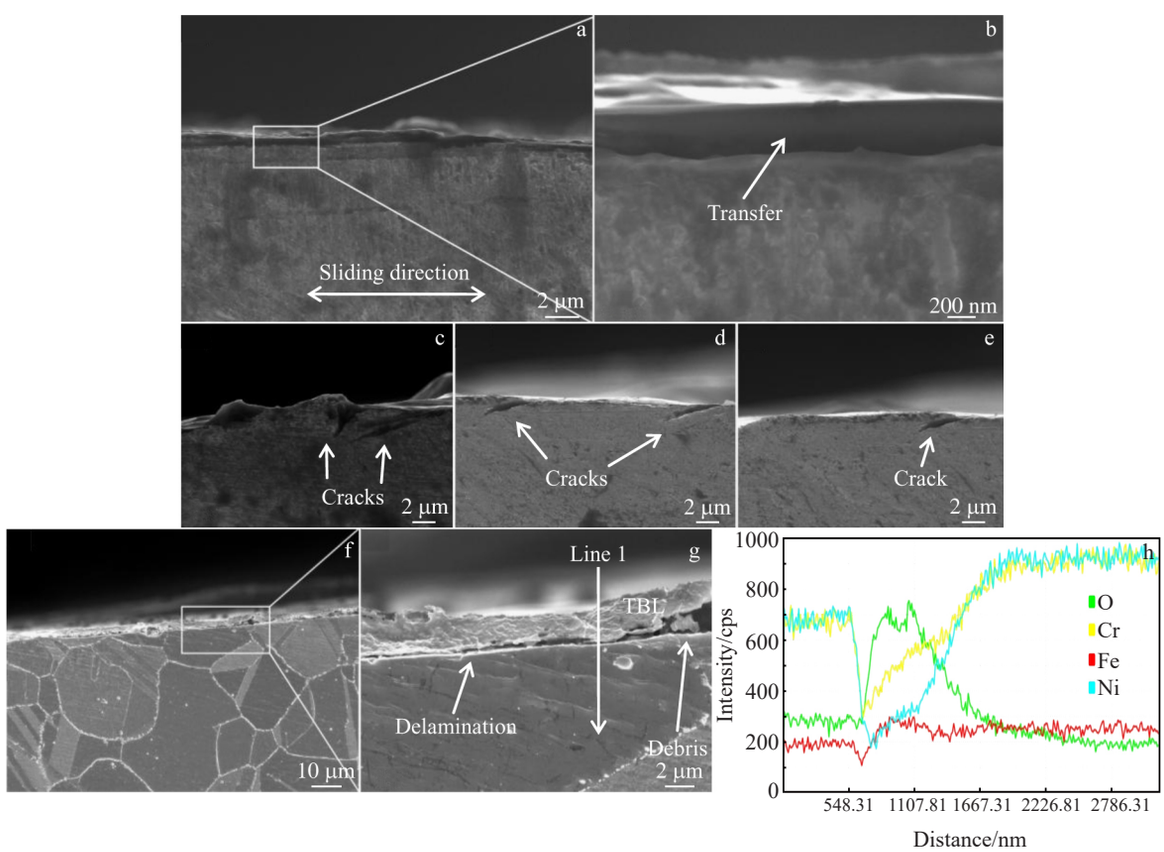

Fig.11 SEM cross-section images of 690 TT alloy tube after 10^5 cycles (a–b), 5×10^5 cycles (c–e), and 2×10^6 cycles (f–g); EDS line scanning results of line 1 in Fig. 11g (h)

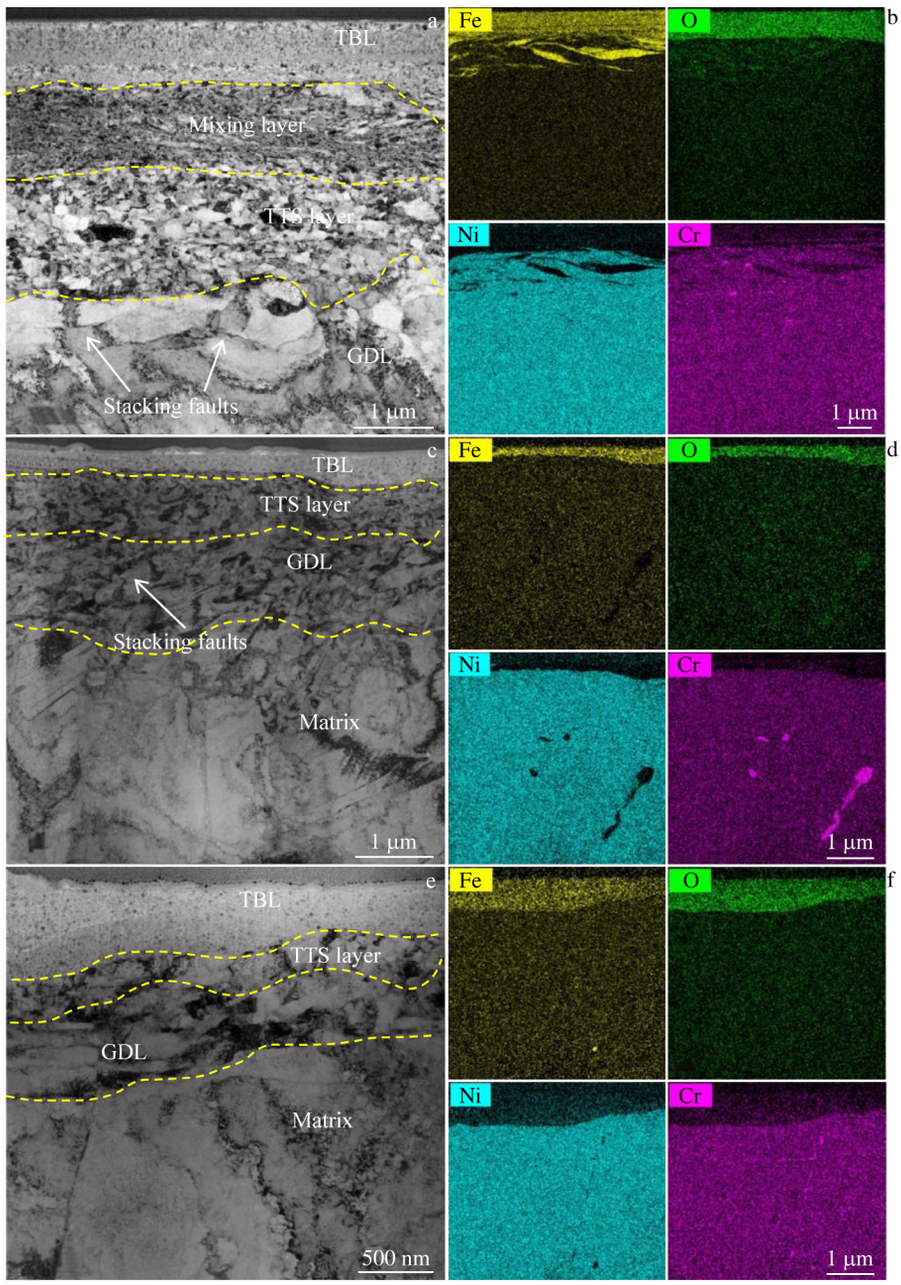

Fig.12 Bright field TEM images (a, c, e) and EDS mappings (b, d, f) of center area of wear marks of 690 TT alloy tube after 10^5 cycles (a, d), 5×10^5 cycles (b, e), and 2×10^6 cycles (c, f)

matrix grains are transformed into the layered structure, and the degree of damage is greater under the same physical action. Therefore, large equiaxed grains are more quickly crushed and transformed into nanocrystals, resulting in a faster process of microstructure evolution and the formation of thicker TTS layer and GDL. When the number of cycles reaches 5×10^5, the wear enters a stable stage, and the rate of delamination and detachment on the surface gradually reaches a dynamic balance with the formation of TTS layer and GDL below the surface. The layered structure begins to dominate in an orderly manner, and the thickness of TTS layer and GDL becomes smaller and tends to stabilize.

No significant difference can be observed in the microstructure between the samples after 2×10^6 and 5×10^5 cycles. As shown in Fig. 12e, TTS layer thickness is approximately 500 nm. Therefore, it is believed that the microstructure evolution enters a stable stage, and the main damage mechanisms at this time are crack propagation and delamination.

Fig. 13c shows SAED pattern of the surface oxide film located at circle area in Fig. 13b. The results indicate the presence of Fe_3O_4 and spinel (Ni, Fe) (Fe, Cr)$_2O_4$ in TBL. According to the point-pH diagrams[18] of Ni, Fe, and Cr in high temperature and high pressure water environments, metals can react with water to form Cr^{3+}, Ni^{2+}, Fe^{2+}, and Fe^{3+}. Cr^{3+} and Ni^{2+} firstly form $Cr(OH)_3$ and $Ni(OH)_2$ in water, but

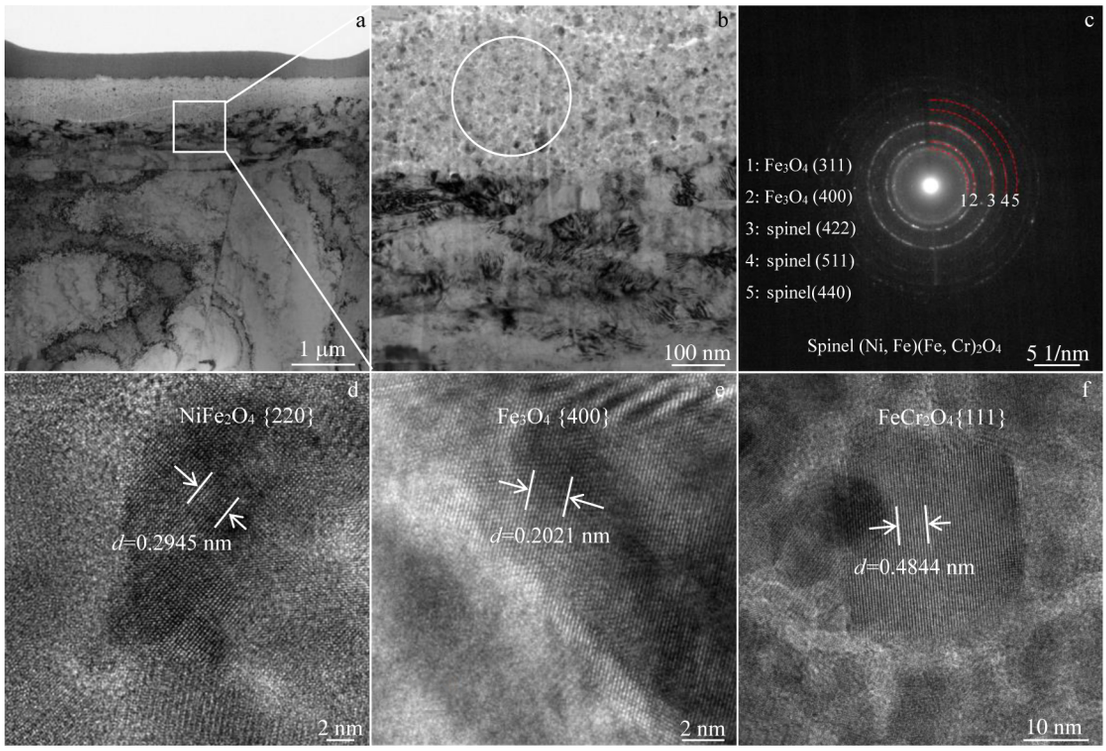

Fig.13 HRTEM images of TBL in 690 TT alloy tube after 2×10^6 cycles (a–b, d–f); SAED pattern of marked circle area in Fig.13b (c)

their hydroxides cannot exist stably in high temperature and high pressure water environment, resulting in the formation of relatively stable Cr_2O_3 and NiO, as shown in Eq. (1 – 2), respectively, as follows:

$$2Cr(OH)_3 \rightarrow Cr_2O_3+3H_2O \quad (1)$$

$$Ni(OH)_2 \rightarrow NiO+H_2O \quad (2)$$

Fig.13d–13f show HRTEM images of TBL in 690 TT alloy tube after 2×10^6 cycles. Through calculation and comparison, it can be determined that Fe_3O_4, spinel $NiFe_2O_4$, and $FeCr_2O_4$ also exist in TBL. The formation of spinel is attributed to the transfer of Fe attached to the surface of 690 TT alloy tube, which forms a large amount of Fe^{2+} and Fe^{3+} and reacts with Cr_2O_3 and NiO to form spinel oxides, as expressed by Eq.(3–5), as follows:

$$NiO+2Fe_3^{+}+6OH^- \rightarrow NiFe_2O_4+3H_2O \quad (3)$$

$$Cr_2O_3+Fe^{2+}+2OH^- \rightarrow FeCr_2O_4+H_2O \quad (4)$$

$$Cr_2O_3+Ni^{2+}+Fe^{2+}+2OH^-+2e^- \rightarrow (Ni, Fe)(Fe, Cr)_2O_4+H_2O \quad (5)$$

After low cycles, the damage degree of the metal surface is relatively slight, and physical factors, such as hardness and stress field, are dominate influence factors. With the experiment further proceeding, the debris is corroded by water, and TBL and delaminated metal on the surface are crushed and adhere to the surface to form an oxide film. The influence of chemical factors, such as temperature and hydrochemical environment, is dominant in this case. The transformation of wear and corrosion mechanisms leads to the thinning of TBL during the transformation process, but ultimately the physical delamination and chemical corrosion processes reach the dynamic equilibrium. Therefore, the thickness of the oxide film firstly decreases, then increases, and finally tends to stabilize.

3 Conclusions

1) The depth contour of the wear marks of 690 TT alloy tube presents the W-shape, whereas that of the 405 SS plate presents the U-shape. The protrusion in the center of wear mark area of 690 TT alloy tube is caused by the material transfer from the 405 SS plate. The protrusion of the edge of the wear mark on surface is caused by the movement and stacking of the transfer material of 405 SS plate along the sliding directions during the reciprocating compression motion.

2) The dominant mechanism of fretting wear during 10^5 cycles is adhesive wear accompanied by a large amount of material transfer, whereas the dominant mechanisms of fretting wear during 5×10^5 and 2×10^6 cycles are crack initiation, propagation, and delamination. Compared with the pure slip conditions, the wear rate under impact wear conditions continues to increase, mainly because the impact action causes surface delamination and detachment, leading to easier corrosion.

3) The main components in TBL are Fe_3O_4, spinel $NiFe_2O_4$, $FeCr_2O_4$, and (Ni, Fe) (Fe, Cr)$_2O_4$. A mixing layer exists beneath TBL in the sample after 10^5 cycles, because the wear does not yet enter the stable stage in the early stage of cycling. The large-sized equiaxed crystals on the surface of 690 TT alloy cannot prevent the invasion and extension of Fe-rich materials in TBL, forming a mixing layer. At the same time, a TTS layer rapidly forms below the mixing layer. The samples

after 5×10^5 and 2×10^6 cycles barely show difference in the cross-section morphologies, and TTS layer thickness is approximately 500 nm. The microstructure evolution enters a stable stage.

References

1 Liu X C, Ming H L, Zhang Z M *et al. Acta Metallurgica Sinica* (*English Letters*)[J], 2019, 32(12): 1437

2 Xin L, Wang Z H, Li J *et al. Tribology Transactions*[J], 2017, 60(5): 913

3 Xin L, Lu Y H, Otsuka Y *et al. Materials Characterization*[J], 2017, 134: 260

4 Ning F Q, Tan J B, Zhang Z Y *et al. Journal of Materials Science & Technology*[J], 2021, 66(7): 163

5 Jeon S H, Song G D, Hur D H. *Scanning*[J], 2018, 2018: 7845176

6 Wang Z H, Lu Y H, Li J *et al. Tribology International*[J], 2016, 95: 162

7 Xin L, Han Y M, Ling L G *et al. Materials*[J], 2020, 13(10): 2417

8 Soria S R, Claramonte S, Yawny A. *Tribology International*[J], 2021, 155: 106803

9 Li J, Lu Y H, Zhang H Y. *Tribology International*[J], 2015, 81: 215

10 Zhang Y S, Ming H L, Tang L C *et al. Tribology International*[J], 2021, 164: 107229

11 Kim J H, Hwang I S. *Nuclear Engineering and Design*[J], 2005, 235(9): 1029

12 Suh N P. *Wear*[J], 1977, 44(1): 1

13 Jahanmir S, Suh N P, Ii E. *Wear*[J], 1975, 32(1): 33

14 Xin L, Yang B B, Li J *et al. Corrosion Science*[J], 2017, 123: 116

15 Ming H L, Liu X C, Yan H L *et al. Scripta Materialia*[J], 2017, 170: 111

16 Rybiak R, Fouvry S, Bonnet B. *Wear*[J], 2010, 268(3–4): 413

17 Feng K L, Shao T M. *Wear*[J], 2021, 476: 203747

18 Huang J B, Wu X Q, Han E H. *Corrosion Science*[J], 2009, 51(12): 2976

高温高压水环境中690 TT传热管冲切双轴微动磨蚀过程中的微观组织演变

周博开，刘　鑫，李　燊，胡　勇

(中国原子能科学研究院，北京 102413)

摘　要：模拟压水堆蒸汽发生器传热管在高温高压水环境下服役，采用690 TT合金管和405 SS板组成的摩擦副进行冲切双轴微动磨蚀实验，研究了冲切微动磨蚀过程中690 TT管的微观组织演变过程。采用白光干涉仪、扫描电子显微镜、透射电子显微镜和拉曼光谱等分析手段对磨蚀表面及近表面的微观组织和磨蚀产物进行探究。结果表明：在10^5次循环以内，690 TT合金的磨损机制主要为伴随材料转移的粘着磨损；5×10^5至2×10^6次循环下，690 TT合金的磨损机制主要为裂纹萌生、扩展和分层脱落。微观组织演变方面，10^5次循环的样品截面微观形貌中，三体层下存在混合层；5×10^5和2×10^6次循环的样品截面微观形貌区别不大，具有厚度约为500 nm的摩擦转化结构层，微观组织演变进入稳定阶段。

关键词：690 TT合金；冲切微动磨蚀；传热管；微观组织演变

作者简介：周博开，男，1999年生，硕士，中国原子能科学研究院，北京 102413，E-mail：954806603@qq.com